Magyarhoni Földtani Társulat
Földtani Közlöny
Hungarian Geological Society

156/2, 99–113., Budapest, 2026

DOI: 10.23928/foldt.kozl.2026.156.2.99

Manganese oxide mineralisation hosted in Upper Triassic dolostone near Királyszentistván, Hungary

Topa, Boglárka Anna[1,2]*, Leskó, Máté Zsigmond[2], Aradi, László[3]; Segui-Fábián, Diego[3]; Kazup, Ágota[4], Kristály, Ferenc[2], Bulátkó-Debus, Délia[2], Weiszburg, Tamás[5], Zajzon, Norbert[2]

[1]Doctoral School of Environmental Sciences, Eötvös Loránd University, Budapest, Hungary; [2]Institute of Exploration Geosciences, University of Miskolc; [3]Archaeometry Laboratory, National Archaeological Institute, Hungarian National Museum Public Collection Centre (HNMPCC), Budapest, Hungary; [4]Institute of Physical Metallurgy, Metal Forming and Nanotechnology, University of Miskolc; [5]Department of Mineralogy, Eötvös Loránd University, Budapest, Hungary
*topabogi@gmail.com
ORCID: Topa Boglárka: https://orcid.org/0000-0003-1996-2261; Leskó Máté: https://orcid.org/0000-0003-1948-2380; Aradi László: https://orcid.org/0000-0003-0276-3119; Kazup Ágota: https://orcid.org/0009-0001-0193-1777; Kristály Ferenc: https://orcid.org/0000-0002-0075-5994; Weiszburg Tamás: https://orcid.org/0000-0001-8183-4434; Zajzon Norbert: https://orcid.org/0000-0003-4664-8091

Mangán-oxidos ásványtársulás a Királyszentistván környéki felső triász dolomitban

Összefoglalás

A Királyszentistván környéki felső triász dolomitban megjelenő mangándús ásványtársulás különleges, fekete, ágasbogas (dendrites) kifejlődésű mangán-oxidjairól vált ismertté, melyeket gyakran sárgásbarna goethitbevonatok tesznek még látványosabbá. Ezek a jellegzetes példányok erősen töredezett és porló dolomittal kitöltött üregekben fordulnak elő, de a mangán- és vasásványok repedések menti bevonatok vagy masszív bekérgezések formájában is jelen vannak a lelőhelyen. A minták ásványos összetételének, valamint szöveti viszonyainak elemzése röntgen-pordiffrakció, pásztázó elektronmikroszkópos vizsgálatok (SEM-BSE felvételek, SEM-EDX pontanalízis és elemtérképezés), mikro-XRF elemtérképezés, Raman-spektroszkópia és komputertomográfia segítségével történt. A vizsgált paragenezist főként csatornaszerkezetű mangán-oxidok (romanèchit, todorokit és a coronaditcsoport ásványai) alkotják, hozzájuk goethit társul. A minták szöveti jellemzése az ásványok szoros, mikroléptékű összenövéseit és jelentős kémiai heterogenitását mutatja, ami a folyamatosan váltakozó redox- és pH-viszonyokat tükröző, többlépcsős ásványkiválásra utal. Az eredmények alapján a komplex ásványtani vizsgálatok – különösen a nagy felbontású szöveti elemzésekkel kiegészítve – alapvető információkat szolgáltathatnak a dolomitrepedésekben zajló fluidum–kőzet kölcsönhatások és a képződési környezetek fejlődésének értelmezéséhez. A királyszentistváni előfordulás ezáltal túlmutat az ásványtani érdekességeken, és jól szemlélteti, hogy a látszólag gyakori ásványtársulások részletes ásványtani vizsgálata hozzájárulhat a helyi földtani és geokémiai fejlődéstörténet pontosabb megismeréséhez.

Tárgyszavak: dolomit, mangán-oxidok, romanèchit, goethit, dendritek

Abstract

A manganese- and iron-bearing mineral assemblage occurring in Upper Triassic dolostone near Királyszentistván (Transdanubian Range, Hungary) was investigated in order to characterise the mineralogical composition and to reveal the textural relations on the micrometre scale, thereby contributing to a better understanding of the geological processes yielding these manganese oxides, partially covered by yellowish-brown goethite, occurring within vugs and cavities containing strongly brecciated and pulverulent dolomite. To analyse the detailed mineralogical and textural features of the samples X-ray powder diffraction, scanning electron microscopy (SEM-BSE imaging, SEM-EDX point analysis and elemental mapping), micro-XRF elemental mapping, Raman spectroscopy and computed tomography were applied. The investigated assemblage consists mainly of tunnel-structured manganese oxides, including romanèchite, todorokite and coronadite-group minerals, associated with goethite. Micrometre-scale observations reveal intimate intergrowths of mineral phases and heterogeneous element distributions, indicating multiple stages of mineral precipitation under changing redox and pH conditions. The results demonstrate that integrated mineralogical investigations, particularly high-resolution textural analyses, provide essential constraints on fluid–rock interaction processes and the evolution of mineralising environments. The Királyszentistván occurrence highlights the geological significance of detailed mineralogical studies of seemingly common mineral assemblages in reconstructing local geological and geochemical processes.

Keywords: dolostone, dolomite, manganese oxides, romanèchite, goethite, dendrites

Introduction

A rather usual mineral assemblage with a very unusual appearance was revealed by collectors in 2019 (Mozgai 2023). Specimens from the dolostone[1] quarry, Királyszentistván (Transdanubia, Hungary), widely referred to as 'romanèchite and goethite', rapidly gained recognition due to their distinctive and highly aesthetic appearance (*Fig. 1*). The black dendritic, coral-shaped branches, covered partially by brownish coating and further enhanced by the light tone of the host rock made the locality famous worldwide. Even in the mindat.org database (Ralph et al. 2025), the page dedicated for romanèchite (https://www.mindat.org/min-3441.html) contains photos of six different specimens from Királyszentistván uploaded by people from all over the world. Thanks to the dedication and enthusiasm of the collectors, the initial identification was performed by various instrumental analytical technics (Kupi 2021a) and these preliminary investigations revealed that detailed characterization of the samples could be of interest not just from the mineralogical, but also from the geological point of view.

Typical dendritic manganese coatings, common in carbonate rocks, is widespread in the quarry on the dolostone surface, and further unique manganese oxide appearance types can be distinguished, too. According to Kupi (2021a, b) the most common forms are tree- or coral-like, black, lustrous aggregates with botryoidal iron oxide(-hydroxide)s developed on them (*Fig. 1)*. These specimens are typically 8–10 cm in size. The largest recovered specimen exceeded 60 cm. Manganese oxides are also present as massive thick black coatings covering the walls of cavities.

The arborescent habit of manganese oxides is very common, and the dendrites are most frequently described as manganese oxide formations, although iron oxide and oxyhydroxide varieties are just as common (Swartzlow 1934). Potter & Rossmann (1979) simply defines manganese dendrites as manganese oxide accumulations exhibiting dendritic pattern. These blackish, tree-like branching motifs usually occur along geological discontinuities, such as bedding planes, joints and fracture surfaces, and they can be found on the surface of rocks and minerals or even within them (Liu et al. 2023, Hou et al. 2025). Manganese dendrites typically appear as quasi-two-dimensional patterns, but rarely three-dimensional structures can also be found (Hou et al. 2025). Based on previous studies (Potter & Rossmann 1979, Ng & Teh 2009, Xu et al. 2010, Hou et al. 2025) manganese dendrites are mostly characterised by tunnel-structured manganese oxide minerals (*Table I*), although Hou et al. (2023) identify a layer-structured manganese oxide (birnessite: $(Na,Ca,K)_{0.6}(Mn^{4+},Mn^{3+})_2O_4$ $1.5H_2O$, monoclinic/triclinic) as the main component of their investigated three-dimensional dendritic samples. The main building blocks of these structures are MnO_6 octahedra (*Table I*) linked by edge-and corner-sharing configurations forming the layer and tunnel structures (Namgung & Lee 2025).

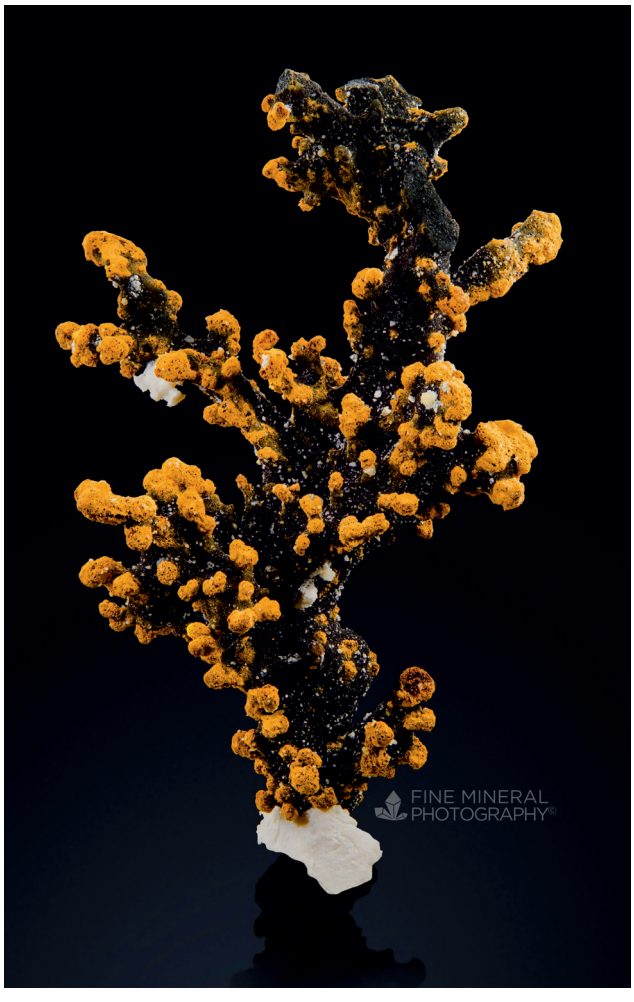

Figure 1. Black branching manganese-oxide specimen from Királyszentistván, partially coated by yellowish goethite. Approximate size: 5×3×2 cm. Collection and photo: László Kupi (Szakáll & Fehér 2025)

1. ábra. *Fekete, dendrites megjelenésű mangán-oxid, részben sárgás goethittel bevonva, Királyszentistvánról. A példány mérete kb. 5×3×2 cm. Gyűjtemény és fotó: Kupi László (Szakáll & Fehér 2025)*

Manganese, characterized by multiple oxidation states (Mn^{2+}, Mn^{3+}, Mn^{4+}), readily responds to environmental changes and therefore precipitates rapidly as micrometre- to submicrometre-scale crystals. This extremely fine grain size already poses difficulties for mineral characterization. Moreover, the precipitates often do not form a single, well-defined distinct mineral, but commonly consist of oriented nanoscale intergrowths and/or mixtures of structurally similar phases – usually with mixed valence features (Namgung & Lee 2025), which are difficult to separate or distinguish from one another. Coherent intergrowth can even occur on the atomic level (Turner & Buseck 1979). The identification is further complicated by the fact that the different tunnel structures can incorporate various cations and water to compensate charge imbalance originating from the mixed valance state of manganese (Post 1999, Namgung & Lee 2025), so chemical analysis without structure-related data is insufficient in most cases.

[1] In this study, the Upper Triassic dolomite host rock is referred to as dolostone to distinguish it from the mineral dolomite.

Table I. Structural units and formulae of various relevant manganese oxides with tunnel structures after TURNER & BUSECK (1981). The numbers indicate the widths of the manganese oxide octahedral chains constraining the tunnels

I. táblázat. *Csatornaszerkezetű mangán-oxidok (coronadit, kriptomelán, hollandit, manjiroit, stronciomelán, romanèchit és todorokit) képlete és építőegységeik TURNER & BUSECK (1981) alapján. A számok a csatornákat létrehozó mangán-oxid oktaéder-láncok szélességét mutatják*

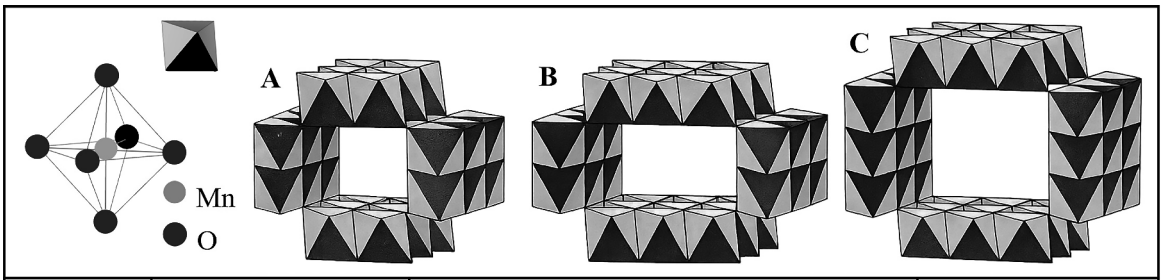

Structure	**Mineral species / abbr.** (WARR 2021)	**Mineral formula** (IMA)	**Structure name** (WANG et al. 2024)
A (2 x 2)	Coronadite / Cor	**Pb**($Mn^{4+}_6Mn^{3+}_2$)O_{16}, monoclinic	α-MnO_2
	Cryptomelane / Cml	**K**($Mn^{4+}_7Mn^{3+}$)O_{16}, monoclinic	
	Hollandite / Hol	**Ba**($Mn^{4+}_6Mn^{3+}_2$)O_{16}, monoclinic	
	Manjiroite / Mji	**Na**($Mn^{4+}_7Mn^{3+}$)O_{16}, tetragonal	
	Strontiomelane / Sml	**Sr**($Mn^{4+}_6Mn^{3+}_2$)O_{16}, monoclinic	
B (2 x 3)	Romanèchite / Rmn	(**Ba**,H_2O)$_2$(Mn^{4+},Mn^{3+})$_5O_{10}$, monoclinic	OMS-6-MnO_2
C (3 x 3)	Todorokite / Tdr	$(Na,Ca,K,Ba,Sr)_{1-x}(Mn,Mg,Al)_6O_{12}\cdot 3\text{-}4H_2O$, monoclinic	Todorokite-MnO_2 / OMS-1-MnO_2

Geological setting

The Királyszentistván manganese oxide locality (*Fig. 2*) is in the central part of the Transdanubian Range, on the SE margin of the Bakony Hills, on the southern limb of the axial syncline, in a position where the Litér thrust repeats the Middle to Upper Triassic sequence (BUDAI et al. 1999). Important tectonic lines are in the vicinity of the site. The Litér thrust runs only few hundred metres WNW from the site and the Herend–Márkó line is to the north (HAAS et al. 2010, HÉJA et al. 2024) (*Fig. 2*).

The Királyszentistván Quarry #1 is located between Királyszentistván and Litér, ca. 10 km east from Veszprém and 5 km north of Lake Balaton. Dolostone and quartz sand were formerly mined in the quarry. The quarry is divided into a WNW part and an ESE part by a steep E–SE dipping fault. The NW half of the quarry reveals the Lower Carnian Kádárta Dolomite Member of the Gémhegy Dolomite Formation (BUDAI & VÖRÖS 2006, BABINSZKI et al. 2023a) with a partially tectonic, partially erosional surface on which Upper Miocene (Pannonian) limnic sand (BABINSZKI et al. 2023b) was deposited covering the ESE part of the quarry. The dolostone has a platform carbonate origin (Cassian Dolomite) (BABINSZKI et al. 2023a). The rock is strongly altered on the southern part of the outcrop. Here not only the NNE–SSW main fault is visible but also a very steep NW–SE structural line crosscutting it at ca. 45°. Along these faults – and especially around their junction – the dolostone is intensely brecciated, weathered, and locally pulverulent occurring as mixed patches and blocks. This zone is a few metres wide. In the joints of tectonic planes and in their surrounding dolostone, the cliffs host vugs and holes from few decimetres to meter-size, partially filled and covered by black and yellowish-brown to brown manganese- and iron-bearing mineral assemblages.

Materials and methods

Samples

Specimens representing different morphological and textural appearances were selected for detailed analysis. Fragments from the selected samples were embedded in a two-component Araldite epoxy resin and polished to obtain flat, even surfaces for further analysis. For bulk mineral identification (X-ray powder diffraction), samples were ground in an agate mortar. *Table II* summarizes the samples with their characteristic features.

Analytical methods

To identify the minerals, characterize the samples in detail, and reveal the detailed micrometre-scale fine textural relations a complex analytical approach was applied.

As a first step, for bulk mineral identification X-ray powder diffraction (XRD) measurements were carried out with a Bruker D8 Discover diffractometer using Cu *K*α radiation

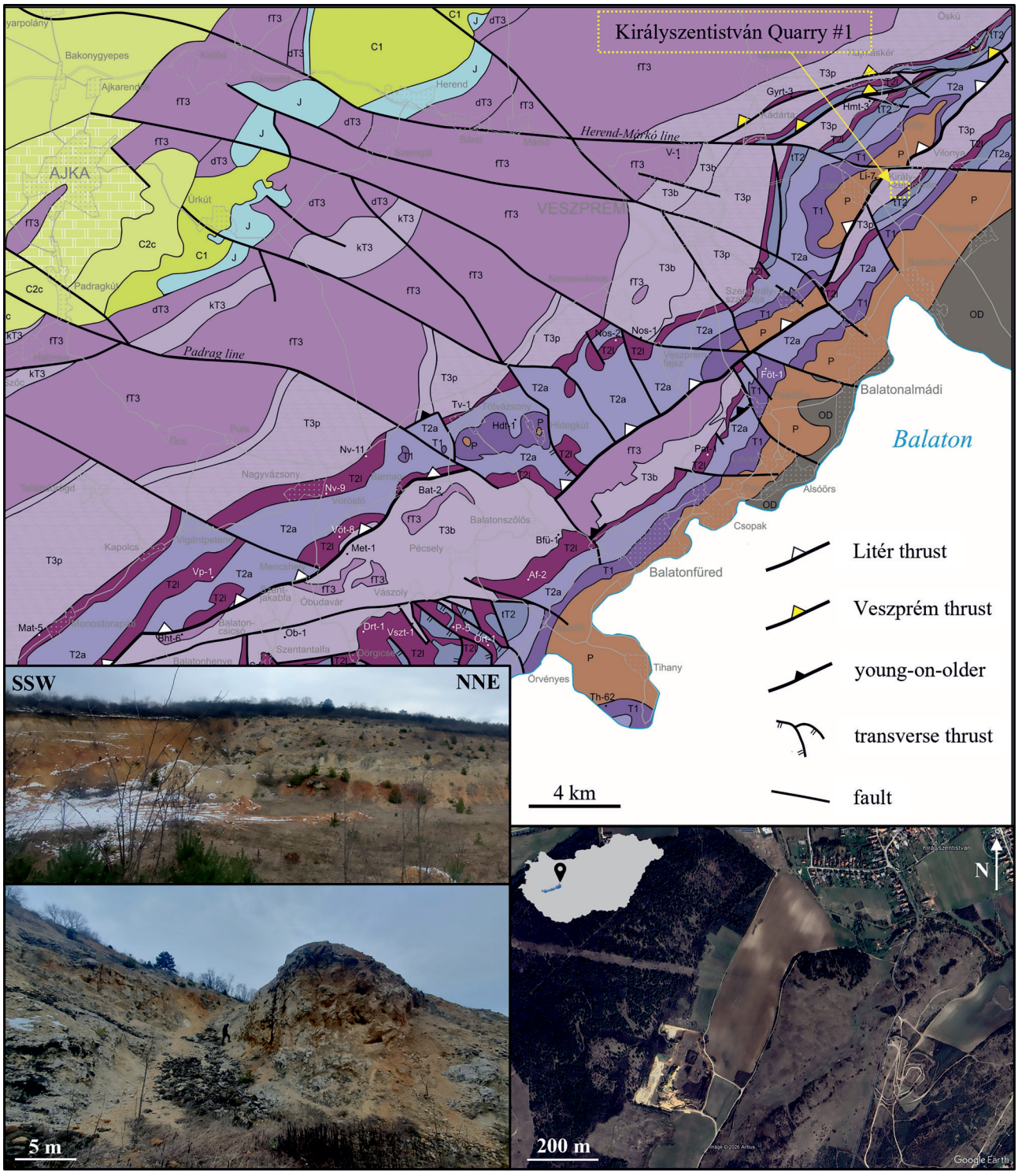

Figure 2. Location of the Királyszentistván Quarry #1 shown in the pre-Cenozoic geological map of the area (after HÉJA et al. 2024) and images of dolostone outcrops in the quarry

2. ábra. *A Királyszentistván I. bánya elhelyezkedése, a környék prekainozoos földtani térképe HÉJA et al. (2024) nyomán, és a bányában feltáródó dolomit*

(40 kV and 40 mA), in the 2–70° 2Θ range, with 0.009° step size and measuring time of 103.2 s.

To explore the micrometre-scale textural features and characterize the chemical composition scanning electron microscopic (SEM) observations (secondary electron (SE) and backscattered electron (BSE) images) and electron beam induced X-ray microanalysis (EDX) (point measurements and mapping) were performed on a Thermo-Fisher Scientific Helios G4 PFIB SEM device, with 15–20 kV accelerating voltage and 13–26 nA probe current.

Texture-related element distributions were further analysed by X-ray fluorescent (XRF) elemental mapping on a Bruker M4 Tornado Plus AMICS 36S micro-XRF device equipped with a rhodium X-ray tube operating at 50 kV ac-

Table II. Sampled specimens and their characteristics with stereomicroscopic images of prepared polished surfaces highlighting some textural features
II. táblázat. *A megmintázott példányok és jellemzőik. Az alsó sor sztereomikroszkópos felvételei a polírozott felszínű minták egyes kiemelt részleteit mutatják*

#1: three-dimensional morphology, branches partially covered with yellowish-brownish coating and dolomite grains	**#2**: three-dimensional thick dendritic morphology among bigger dolomite clasts	**#3:** black and brown / yellowish-brownish thick, layered coatings on the wall of veins and cavities	**#4:** black and brown thick, layered coating, blade- and sponge-like covering on the wall of veins and cavities
			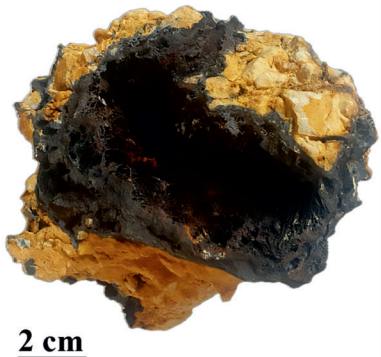
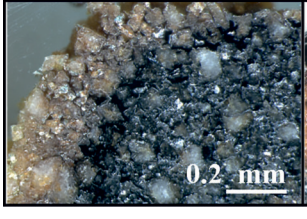	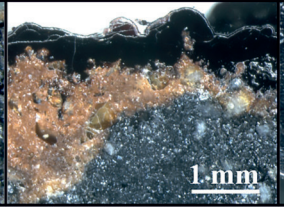	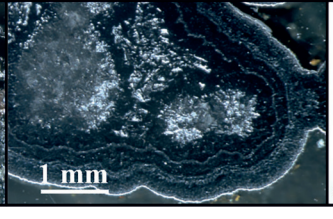	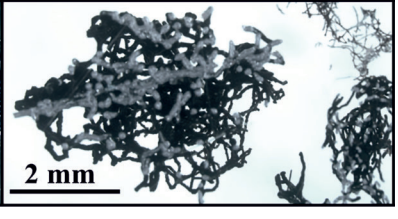

celeration voltage and 600 µA current. Mapping was done with a resolution of 5 and 15 µm beam diameter at 2 mbar pressure.

"In-situ" phase determination was done with Raman spectroscopic measurements on a Renishaw inVia Qontor Raman microspectrometer. The samples were illuminated with a diode-pumped solid-state laser. The excitation wavelength was 532 nm (green) with 0.5 mW power on the surface. To focus the laser on the sample a Leica 100× (N.A. = 0.85) objective was used. The optical grating was 1200 grooves/mm. Measurements were performed using variable exposure times to obtain the best possible signal-to-noise ratio. To identify phases based on their Raman spectra the RRUFF database (Lafuente et al. 2016) and publications of Julien et al. (2004), Bernardini et al. (2019, 2020, 2024, 2025), Post et al. (2020, 2021), Vermeersch et al. (2023) and a reference sample set (Topa et al. 2018) were used.

3D textural relations were analysed by computed tomography (CT). The measurements were carried out with a YXLON FF35 micro-CT system. Imaging was performed at 155 kV and 455 µA. The reconstructed 3D volumes have a spatial resolution of 14.2 µm in all three dimensions, with a magnification of 18.66×. Data visualization and evaluation were done with the VGStudio MAX 3.3 software.

XRD, SEM and CT analyses were performed in the 3DLAB at University of Miskolc. XRF mapping and Raman spectroscopy were carried out in the Archaeometry Laboratory of the HNMPCC National Archaeological Institute.

Characterization of the samples

Mineralogical features

Bulk analysis of the samples by XRD revealed the presence of dolomite ($CaMg(CO_3)_2$, trigonal), quartz (SiO_2, trigonal), goethite (FeO(OH), orthorhombic) and different manganese oxides with minor amount of amorphous or poorly crystalline phases (*Fig. 3*). Romanèchite, todorokite and minerals of the coronadite group can be identified in the diffraction patterns although according to Post (1999) species-level identification of many manganese oxides with XRD only is hindered by their structural similarities causing overlaps of the peaks.

SEM-BSE imaging revealed strong contrast variations among manganese-bearing mineral phases, reflecting substantial chemical heterogeneity among them (*Figs 4, 6, 8*). SEM-EDX point analyses, elemental mapping and XRF mapping indicate that barium (Ba) is the dominant cation incorporated into the manganese oxide structures (*Figs 4–6*), occurring with highly varying concentrations (from ~8 to ~17 wt%). In addition to Ba, sodium (Na), magnesium (Mg) aluminium (Al), silicon (Si), potassium (K), calcium (Ca), iron (Fe), cobalt (Co) and vanadium (V) are also detected in variable amounts. Ba-poor oxide phases exhibit elevated levels of Na, K, Mg, Ca (*Fig. 6*) and occasionally lead (Pb) or strontium (Sr), whereas Ba-rich phases consistently contain vanadium (V). Goethite is characterised by no

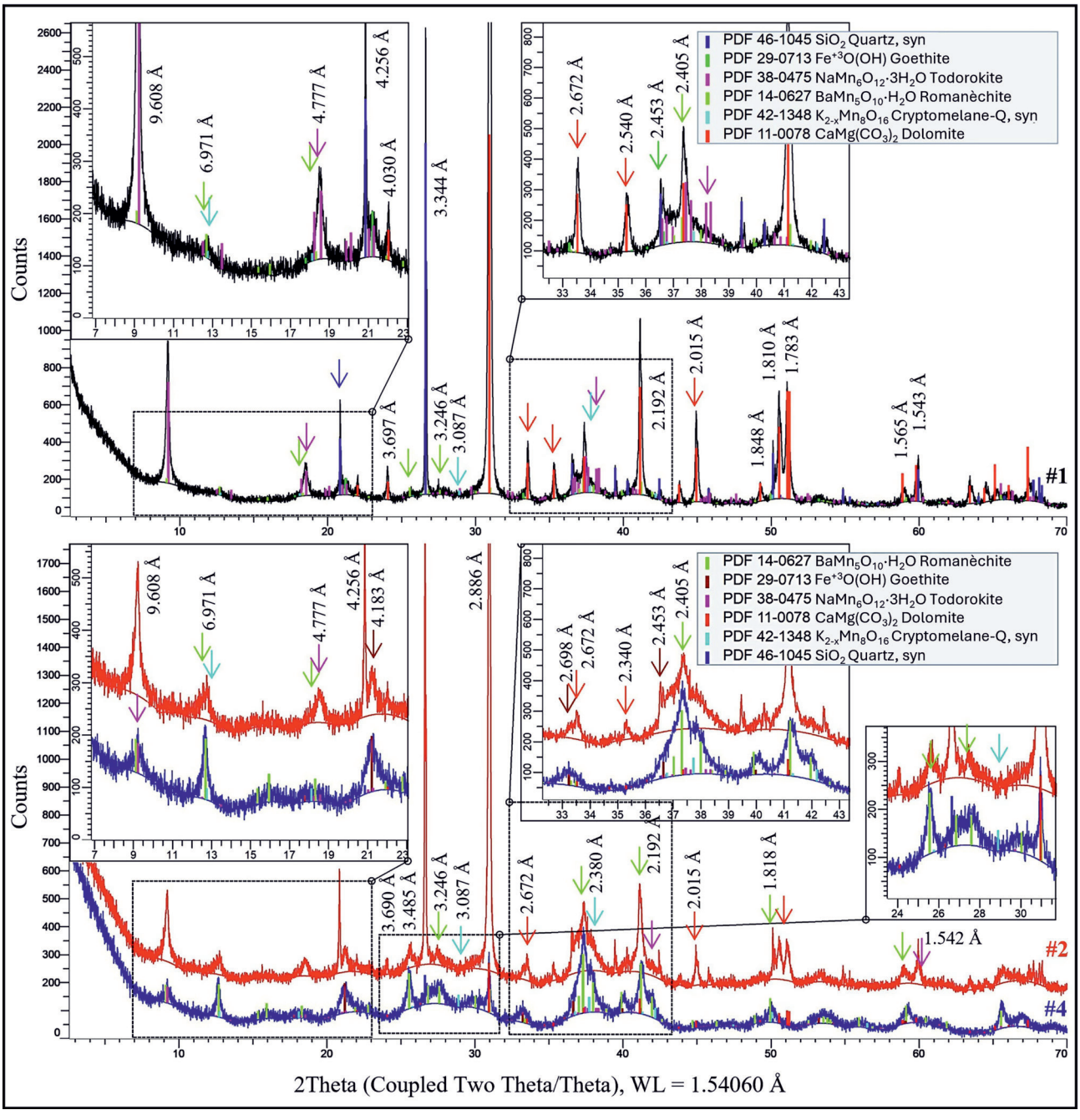

Figure 3. Representative X-ray powder diffraction patterns from samples #1, #2, #4 with the d-values of the main peaks

3. ábra. *Az #1, #2 és #4 minták reprezentatív röntgen-pordiffraktogramjai a fő csúcsokhoz tartozó d-értékekkel*

traceable presence of Ba and K while Co (*Fig. 4*) and Si (*Figs 4, 6, 8*) show elevated concentrations occasionally together with chlorine (Cl) and copper (Cu).

Raman spectroscopic measurements show the presence of romanèchite, todorokite and coronadite-group minerals (*Fig. 7*). However, the intimate micrometre-scale intergrowth of the phases resulted in mixed Raman spectra showing characteristic bands for several mineral species in most cases (*Fig. 8*). The intensity of certain peaks shows orientation-dependent variations among the spectra. On *Fig. 7* Raman bands occurring around 150 and 208 cm^{-1} correspond to romanèchite, meanwhile in the region between them around 180 cm^{-1} peaks of coronadite group minerals are present. Peaks around (and below) 130 cm^{-1} belong to todorokite. The region marked by light blue colour around the peak at 291 cm^{-1} is characteristic for both romanèchite and todorokite. The region marked around 512 cm^{-1} usually occurs in the coronadite group, todorokite and subordinately in romanèchite and seems to be highly influenced by orientation. Green highlighted Raman bands around 585 cm^{-1} also belong to all three structures but highly vary in intensity according to changes in orientation. In the region characterised by the dashed lines at 629 cm^{-1} and 739 cm^{-1} the bands show variations both in intensity and position de-

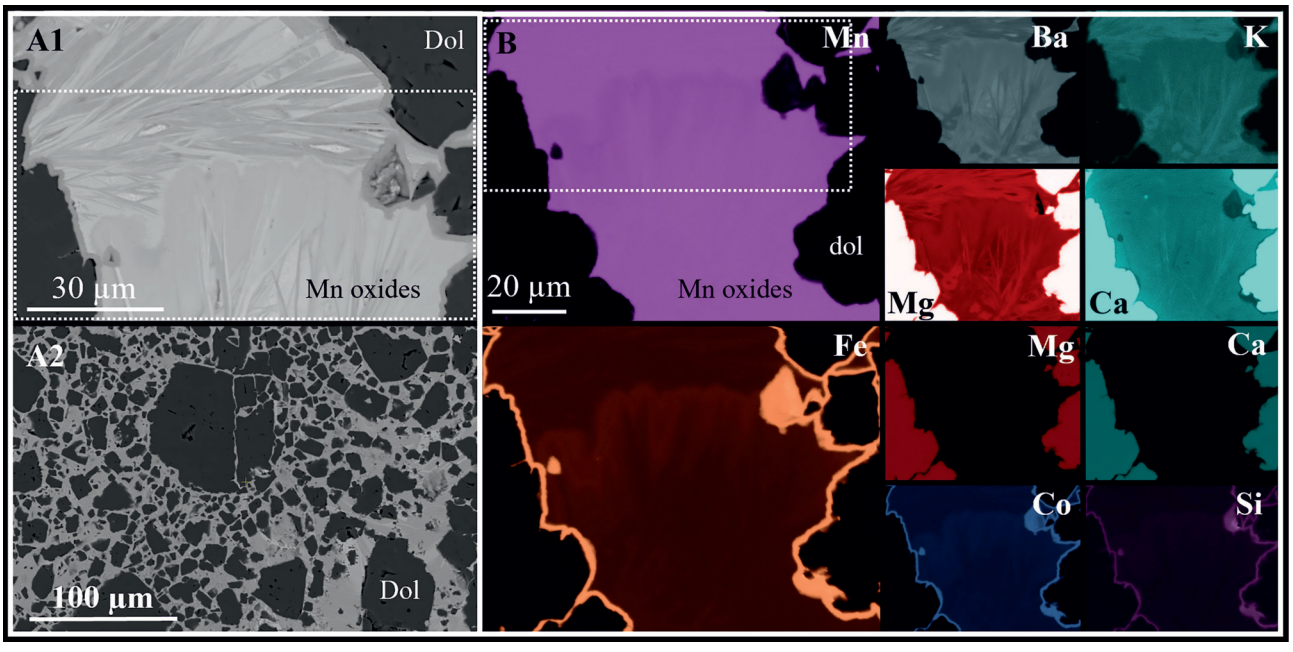

Figure 4. Selected area of sample #2 showing manganese oxides and goethite textural relations among dolomite grains on (A1, A2) SEM-BSE images (enlarged, overview) and (B) SEM-EDX elemental maps. White dashed rectangles show the same area. White letters in the top right corners indicate the mapped elements. Within each map, brighter shade indicates higher concentration. Black letters in bottom left corners indicate enhanced Mg and Ca maps to counterbalance the effect caused by the presence of dolomite ($CaMg(CO_3)_2$) grains. Brecciated dolomite grains of 5–100 µm are coated by a ca. 3 µm goethite rim (concentrating Co and Si). The rest of the intergranular space is filled by manganese oxides (concentrating Ba and K, too) and goethite.

4. ábra. *Mangán-oxidos és goethites mátrix a dolomitszemcsék között a #2 mintában. (A1, A2) nagyított és áttekintő SEM-BSE-felvételek, (B) SEM-EDX-elemtérképek. A fehér szaggatott téglalapok az azonos területeket jelölik. A fehér betűk a jobb felső sarokban az elemeket jelzik. Egy térképen belül a világosabb árnyalat nagyobb koncentrációt mutat. A bal alsó sarokban fekete betűk jelölik az eredeti Mg- és Ca-térképek felerősített változatait, melyek a dolomit ($CaMg(CO_3)_2$) szemcsék hatását ellensúlyozzák. A ~5–100 µm-es töredezett dolomitszemcséket körülvevő ~3 µm-es goethitszegélyben Co és Si dúsul. A szemcsék közötti teret Ba- és K-tartalmú mangán-oxid ásványok keveréke és goethit tölti ki.*

pending on the presence of romanèchite, todorokite and the coronadite-group minerals in the analysed points since all structures have lattice vibrations in those regions.

Textural features

Dolomite grains ranging from a few micrometres up to a few hundred micrometres can occur both on the surface of the samples and included within the oxides. Textural observations show that the dolomite fragments are surrounded by manganese oxides. (*Figs 4, 9*). The grain fragments are usually angular. The cracks along these dolomite fragments are sometimes also filled by manganese oxides. In some parts of the samples, individual dolomite grains are coated by an approximately 3 µm thick rim of goethite (*Figs 9–10*). The distribution of the goethite-encrusted and non-coated dolomite grains shows heterogeneity within the sample (*Fig. 9*).

Based on computed tomography, the distribution of the dolomite grains within the manganese oxide matrix is even in all directions of the studied specimens *(Fig. 11)*. CT analysis also allowed to follow the changes of textural relations through a solid dolostone sample surrounded and infiltrated by manganese mineralisation. Manganese oxides partially filled the cracks and fissures, precipitated on the surfaces and in suitable voids they grew dendritic 3D structures embedding the dolomite grains (*Fig. 11*).

Manganese oxides occur in at least three different textural position. In the branchlike "three-dimensional" dendritic forms, according to higher resolution SEM imaging and SEM-EDX mapping the manganese-bearing phases surrounding the dolomite grains show a finely interwoven texture on the micrometre scale (*Fig. 4)*.

Samples from the massive, manganese-bearing coatings, which macroscopically appear homogenous, generally do not contain dolomite grains. On the micromere scale these Mn-rich coatings exhibit heterogeneous textural and mineralogical features (*Figure 5*). Manganese oxides occur in void-filling positions, too.

The intimate intergrowth of the different manganese oxide minerals (romanèchite, hollandite and todorokite) commonly alternates with goethite, even on the micrometre-scale (*Fig. 6*).

Goethite can also be characterised by different morphological and textural features in the mineral assemblages. Besides the macroscopically well-discernible yellowish-brown coating on the surface of the dendritic manganese oxides, goethite and iron oxyhydroxides with different level of crystallinity also occur in the form of velvety black thin layers on manganese oxide surfaces, or even with a sponge-like, filamentous interwoven texture (*Table II*). Sometimes the voids among these nets of delicate fragile threads are also filled by manganese oxides (*Fig. 6*). Colloform and botryoidal goethite encrustations

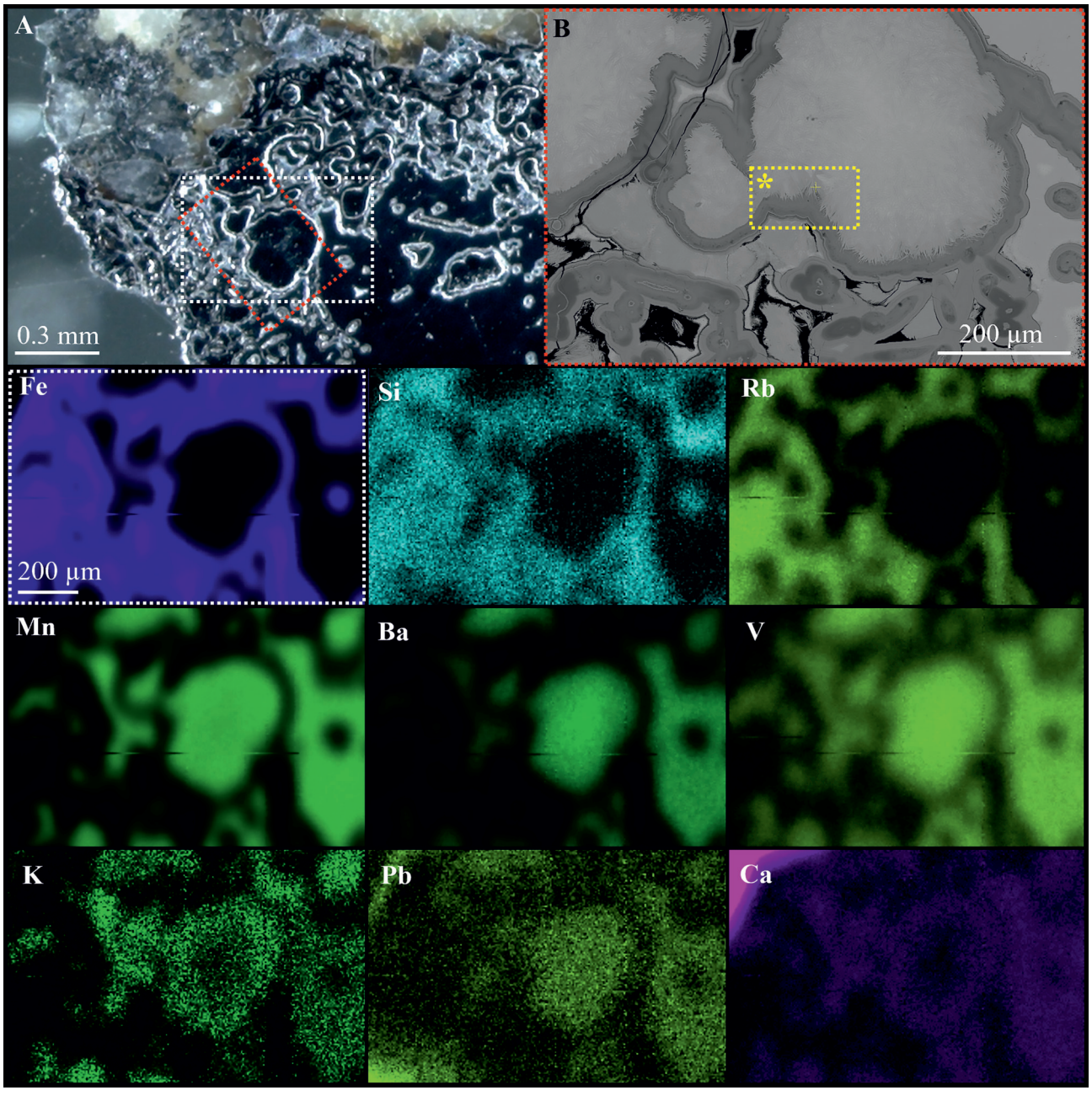

Figure 5. Dolomite-free, manganese oxides and goethite-bearing area of sample #4. (A) Stereomicroscopic and (B) SEM-BSE images (enlarged into the area marked by red dashed rectangle) with micro-XRF elemental maps (enlarged into the area marked by white dashed rectangle). White letters indicate the mapped elements. Within each map brighter shade indicates higher concentration. The white rectangle with the asterisk (*) marks the area shown in *Fig. 8*. Si and Rb occur within goethite, while Ba, V, K Pb and Ca are present in the manganese-oxides

5. ábra. *A #4 minta egy dolomitmentes, mangán-oxidos és goethites területe (A) sztereomikroszkópos és (B) SEM-BSE-felvételeken mikro-XRF-elemtérképekkel. A fehér betűk a bal felső sarkokban az elemeket jelzik. Egy térképen belül a világosabb árnyalat nagyobb koncentrációt mutat. A csillaggal (*) jelölt téglalap a* 8. ábra *helyét jelöli. A Si és Rb a goethitben dúsul, míg a Ba, V, K, Pb és Ca a mangán-oxid-fázisokban jelenik meg*

are also characterised by rhythmic morphological and chemical zonation (*Figs 6, 8*).

Discussion

The observations indicate that specimens from Királyszentistván contain a wider range of minerals in the assemblage than it seemed at first glance. The appearance of the black dendritic romanèchite is aesthetically amplified by the presence of a yellowish-brown goethite coating. Furthermore, besides this surface coating, goethite is also present intermixed with other phases, which can only be recognized by microscopic methods. In addition, romanèchite is accompanied by other tunnel-structured manganese oxides of elevated Ba content, like todorokite and members of the coronadite group (most probably hollandite). Although the complex analytical approach revealed the presence of dif-

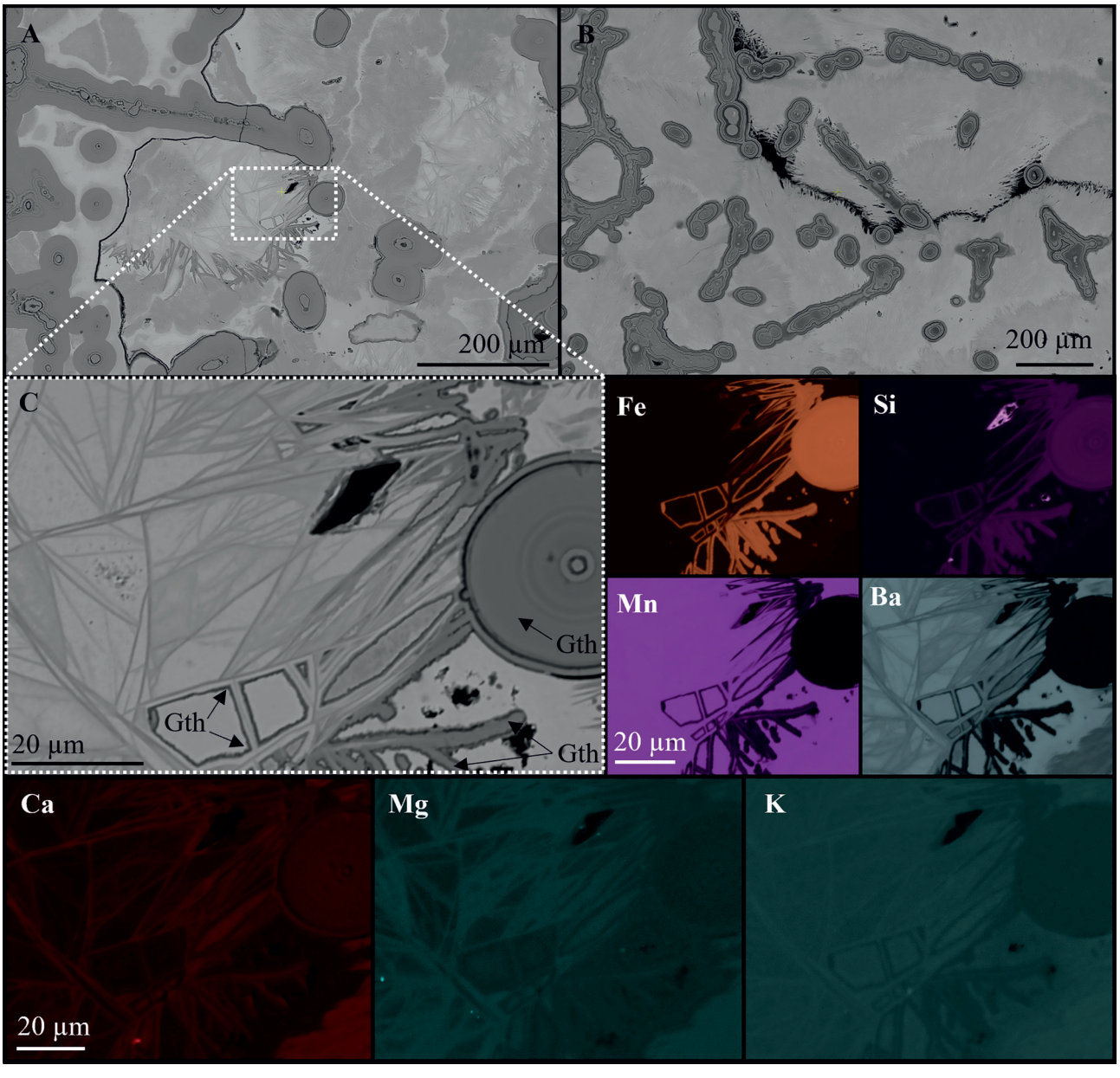

Figure 6. Manganese oxides and goethite in a dolomite-free part of sample #4. (A, B, C) SEM-BSE images and SEM-EDX elemental maps illustrate the chemical heterogeneity and textural complexity. White letters indicate the mapped elements. Within each map brighter shade means higher concentrations. "Gth" abbreviation stands for goethite (Warr 2021). (A and B) show the relations of manganese oxides and goethite on different scales. (C) reveals the micrometre-scale chemical heterogeneity and the close textural relations of manganese oxides and goethite within the enlarged area of (A)

6. ábra. *Mangán-oxidok és goethit a #4 minta egy dolomitmentes területén. A SEM-BSE-felvételek és a SEM-EDX-elemtérképek szemléltetik a kémiai heterogenitást és a szöveti komplexitást. A fehér betűk az elemeket jelzik. Egy térképen belül a világosabb árnyalat nagyobb koncentrációt mutat. A „Gth" rövidítés a goethitet jelöli Warr (2021) nyomán. (A és B) mangán-oxidok és goethit szöveti viszonya különböző léptékeken. (C) Kémiai heterogenitást mutató mangán-oxidok és goethit mikrométeres léptékű szöveti viszonyai az (A) felvétel kijelölt, nagyított területén*

ferent tunnel-structured manganese oxide minerals, the delicate, micrometre-scale intergrowth strongly hinder the species-level identification. However, SEM-BSE images, SEM-EDX and micro-XRF elemental maps seem to be effective tools to observe the textural relations and track the precipitation sequences, hence mapping can highlight the boundaries even among phases that cannot be separately measured by point analysis with SEM. The relation of manganese oxide minerals and goethite in the samples suggests a rather complex and continuously changing formation environment and fluctuations in the redox and / or pH conditions. Textures represented by *Fig. 6* show that while manganese oxides fill the voids among separately and intactly evolved goethite formations, goethite also occurs as fine encrustation on the surface of submicrometre-scale manganese oxides. This is similar to the case of the dolomite-bearing samples where goethite most commonly appears not just around the dolomite grains (*Figs 8, 9*), but also together with the manganese oxides building up the matrix that cements the dolomite grains.

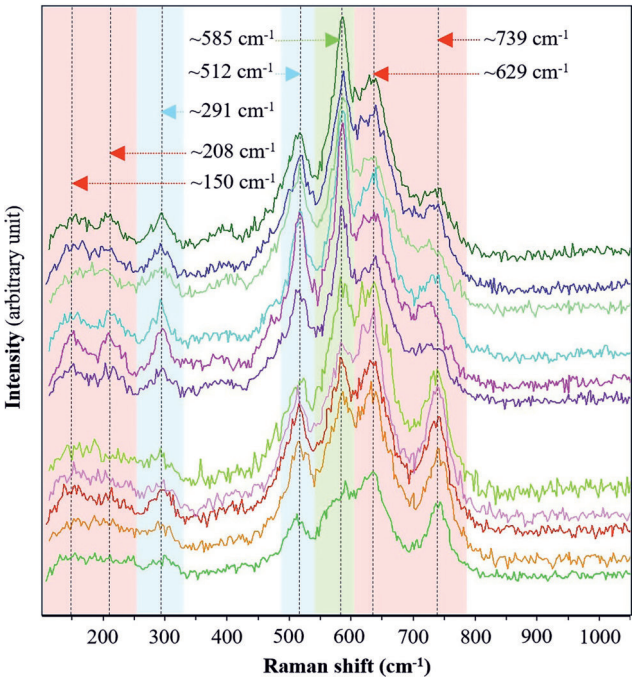

Figure 7. Some Raman spectra obtained from the samples. Background shaded with different colours show the main characteristic bands for the presented tunnel-structured manganese oxides. The black dashed lines indicate the positions of the listed cm^{-1} values serving as a reference for peak shifts

7. ábra. *A vizsgált minták Raman-spektrumai. A különböző színekkel kiemelt háttér a mintákban jelenlevő csatornaszerkezetű mangán-oxidok jellemző Raman-sávjait szemlélteti. A fekete szaggatott vonalak a cm^{-1} értékek pozícióját jelölik, amelyek a csúcseltolódások referenciaértékeiként szolgálnak*

Depending on textural relations, at least three different types of growth forms can be identified in the examined samples. The characteristic three-dimensional dendritic type specimens (Type 1) typically consist of dolomite grains cemented by at least two types of manganese oxides together with goethite. The formation of these structures appears to be controlled by the presence of vugs or cavities in the dolostone filled with loose brecciated and pulverulent dolomites, providing a suitable medium for crystals growth. When the cavities are sufficiently large but empty, only massive encrustations (Type 2) develop on the walls of these cavities, composed of both manganese oxides and iron oxyhydroxides. In contrast, in smaller cavities and wider fractures, manganese oxides and goethite fill the entire available space (Type 3). 3D manganese oxides previously described in literature also suggest that some kind of medium is needed to facilitate the growth towards all directions. Hou et al. (2023) described an unusual manganese mineralisation where 3D dendrites developed within clinoptilolite tuff, while dendritic agate (Çalık & Arzoğullari 2014) and dendritic opal also show three-dimensional dendritic morphology of manganese oxide minerals embedded in them (Hou et al. 2025).

The tectonic lines (and nearby fractures associated with them) provide highly efficient pathways for fluid migration within the dolostone, which is relatively impermeable and more difficult to dissolve than other – calcite-containing – carbonate rocks. The observed tectonized and altered zone

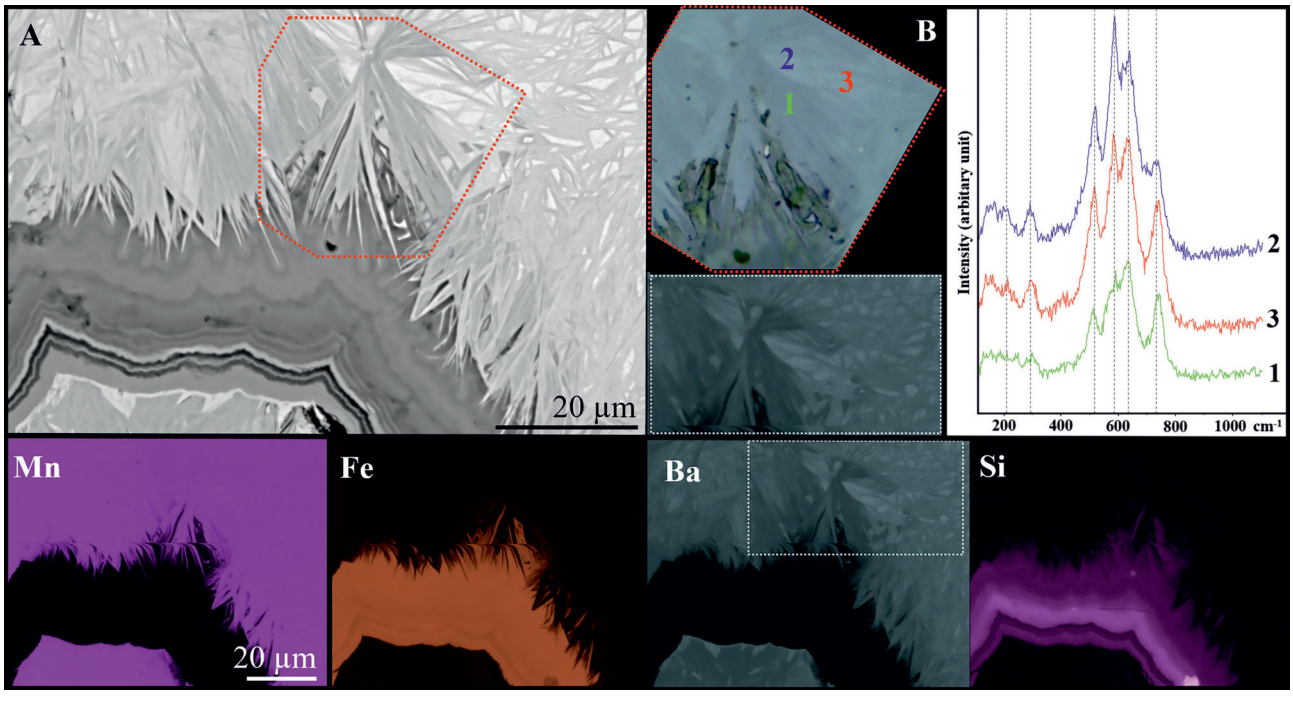

Figure 8. Enlarged area from *Figure 5* (sample #4) marked by the yellow asterisk (*) there, showing manganese oxides and goethite on (A) SEM-BSE and (B) reflected light microscopic images of the area marked by the red dashed polygon with SEM-EDX elemental maps showing the chemical heterogeneity of manganese oxides and goethite. White letters in the top left corners indicate the mapped elements. Within each map brighter shade means higher concentration. Colour numbers show the spots of Raman microspectroscopic analysis of manganese oxides with the corresponding spectra.

8. ábra. *Az* 5. ábra *(#4 minta) sárga csillaggal (*) jelölt nagyított, mangán-oxidos és goethites területe (A) SEM-BSE-felvételen és a piros szaggatott sokszöggel jelzett terület (B) ércmikroszkópos fényképén SEM–EDX-elemtérképekkel, melyek a mangán-oxidok és a goethit kémiai heterogenitását mutatják. A fehér betűk a bal felső sarokban az elemeket jelzik. Egy térképen belül a világosabb árnyalat nagyobb koncentrációt mutat. A színes számok a mangán-oxidok Raman-mikrospektroszkópos elemzési pontjait és a hozzájuk tartozó spektrumokat jelölik.*

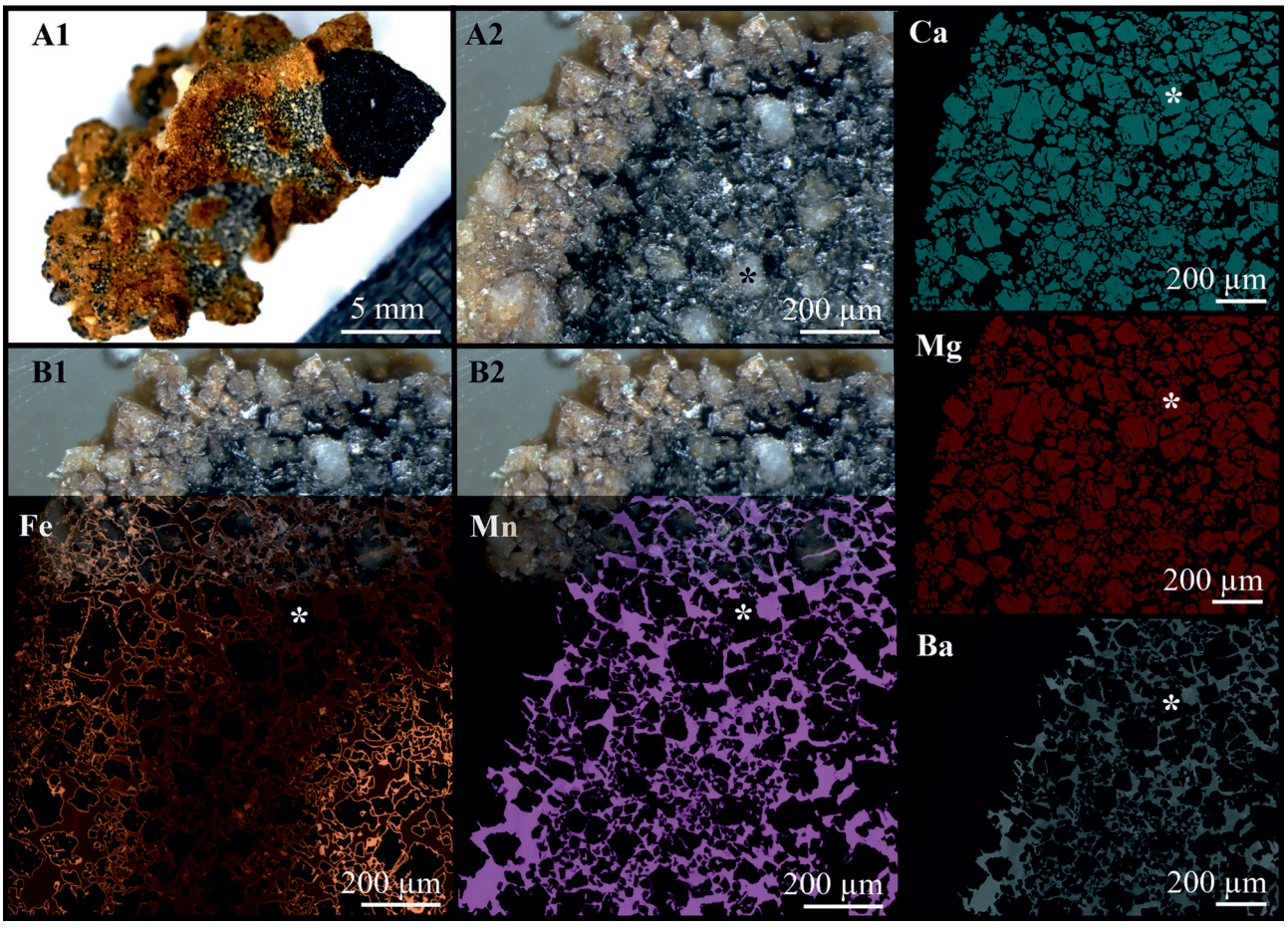

Figure 9. A fragment (sample #1) of a typical specimen from Királyszentistván. Stereomicroscopic images (A1, A2) and SEM-EDX elemental maps show dolomite grains (maps: Ca, Mg) cemented by manganese oxides (maps: Mn, Ba) and surrounded by goethite (map: Fe). Composite pictures (B1, B2) show the textural distribution of Mn and Fe among the dolomite grains. Asterisks (*) highlight the same dolomite grain. White letters in the top left corners indicate the mapped elements. Within each map brighter shade means higher concentrations

9. ábra. *Egy jellegzetes királyszentistváni példány töredéke és a belőle készült #1 minta egy területe. A sztereomikroszkópos felvételek (A1, A2) és SEM–EDX-elemtérképek a mangán-oxidokkal (térképek: Mn, Ba) cementált dolomitszemcséket (térképek: Ca, Mg) mutatják, melyeket goethit vesz körül (térkép: Fe). A kompozitképek (B1, B2) a Mn és Fe szöveti eloszlását mutatják a dolomitszemcsék körül. A csillag (*) egyazon dolomitszemcsét jelöl. A fehér betűk a bal felső sarkokban az elemeket jelzik. Egy térképen belül a világosabb árnyalat nagyobb koncentrációt mutat*

of the dolostone in Királyszentistván likely served as an excellent pathway to metal-containing (Mn, Fe, Ba) fluids, further facilitating dolostone dissolution and the coeval precipitation of manganese and iron oxide phases. The faults visible in the quarry are likely connected to nearby important structural lines like the SW–NE trending Litér-line or the W–E trending Herend–Márkó line, which has likely been active since Eoalpine movements (Tari & Horváth 2010). The Herend–Márkó line was formed as thrust "tear" fault coeval with the Cretaceous Eoalpine deformation (Fodor et al. 2017). The elements required for the formation of the mineral assemblage were likely supplied either locally – such as Ca and Mg released during dolostone dissolution – or introduced by migrating fluids that transported Mn, Fe, K, and Ba. The dissolution of carbonate rocks acts as an effective redox barrier, promoting the precipitation of metal-bearing phases (sulphides and oxides) when dissolved metals are present in the circulating fluids (Robb 2004).

Considering the formation, significance, and Cretaceous activity of the Litér thrust and Herend–Márkó faults, together with the broader geological evolution of the Transdanubian Range, multiple scenarios can be proposed for the origin of the Mn oxide mineral assemblage at Királyszentistván. Just by the presence of manganese and iron mineralisation, the precipitation could have resulted either from cold, descending oxidising meteoric waters during surface weathering, or from ascending hot (or at least warm) brines circulating in the tectonic channels. Additionally, according to Carmichael et al. (2017) and based on Nicholson (1992) the cobalt content of the samples and the Mn-Ba association suggest a supergene terrestrial origin, although the extremely high amount of Ba could be an indicator of hydrothermal fluid contribution, too. The dissolution of dolostone causes continuous shifts in redox and pH conditions, creating a favourable environment for the simultaneous precipitation of manganese and iron oxide minerals. One notable form of the Mn miner-

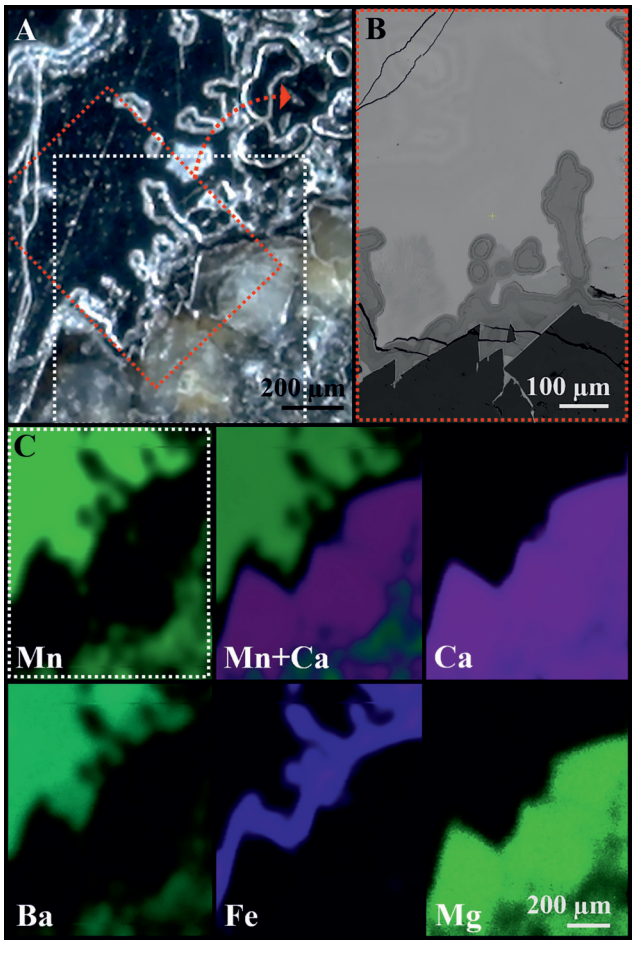

Figure 10. Selected area of sample #4. (A) Stereomicroscopic and (B) SEM-BSE image (45° clockwise rotated and enlarged part of the red dashed rectangle) with (C) micro-XRF elemental maps (area marked by dashed white rectangle). Goethite rim (Fe map) appears around dolomite (Ca and Mg maps) surrounded by manganese oxides (Mn and Ba maps). White letters in the bottom right corners indicate the mapped elements. Within each map brighter shade means higher concentrations. The "Mn+Ca" image is a composite map

10. ábra. *A #4 minta egy kiválasztott területe. (A) Sztereomikroszkópos és (B) SEM-BSE-felvétel (a piros szaggatott téglalappal jelölt terület 45°-kal elforgatott képe) (C) mikro XRF-elemtérképekkel kiegészítve (a fehér szaggatott téglalappal jelölt területről). A mangán-oxidok (Mn és Ba térképek) és a dolomit (Ca és Mg térképek) között kirajzolódik a goethitperem (Fe térkép). A fehér betűk a bal alsó sarkokban az elemeket jelzik. Egy térképen belül a világosabb árnyalat nagyobb koncentrációt mutat. Az „Mn+Ca" térkép kompozit kép*

alisation at Királyszentistván is the development of three-dimensional Mn oxide structures within channels, cavities, and zones filled with pulverised dolomite. This makes the formation of pulverulent dolomite also a relevant question. Pulverulent dolomite was likely not formed exclusively mechanically by tectonism, as not all fault zones created pulverulent dolomite. It needs interaction with water; thus, the tectonism could only be a prerequisite to create pathways for waterflow.

Nagy (1979) describes that during the process of dolomite pulverisation the primary texture of the rock becomes loosened and disrupted. Thus, dolomite pulverisation refers to the process in which intact, hard dolostone transforms into dolomite powder through the disintegration of its original fabric. However, it is well known that the end product of this process is not always powder; but between the fresh rock and the fully pulverised dolomite, a very common transitional brecciated material also develops just like in Királyszentistván. The formation of pulverulent (or pulverised or powdered) dolomite can be associated with ascending hydrothermal fluids (Esteban et al. 2009) while infiltration of meteoric water enhanced by cryogenic mechanical weathering can also affect the powderisation of dolostones (Poros et al. 2013). Reliable identification of the formation processes of both pulverulent dolomite and the manganese and iron oxide mineralisation of Királyszentistván needs further research. More detailed mineralogical (e.g., species-level identification by transmission electron microscopy) and geochemical investigation could serve as a base to better understand and interpret the local geological processes. According to Vasconcelos et al. (1992) and Dekoninck et al. (2023) age determination based on potassium-bearing tunnel-structured manganese oxide can be feasible, which raises the possibility of argon–argon ($^{40}Ar/^{39}Ar$) dating of the Királyszentistván samples, providing additional constraints on the geological evolution at the locality.

Conclusion

Analysis of the manganese- and iron-bearing mineral association of Királyszentistván revealed the presence of at least three types of different manganese oxides (romanèchite, todorokite, coronadite-group minerals) and iron oxyhydroxides (mainly goethite) showing micrometre-scale textural relations. For species-level identification of each phases transmission electron microscopic research would be necessary. $^{40}Ar/^{39}Ar$ dating of manganese oxides could also serve as a base for further research.

Microscale mineralogical investigation of seemingly ordinary mineral assemblages – such as manganese dendrites – can significantly contribute to a deeper understanding of geological and environmental processes not just on a local scale.

Macroscopically hidden fine-textural relations of different manganese and iron oxide(hydroxide)s serve as a good base to track the changes in the redox-pH conditions of the system.

The samples from Királyszentistván clearly demonstrate the significant value of collaboration between people from different fields of mineralogy. Making these specimens accessible to museums and research institutions not only helps to improve comprehensive understanding of the local geological processes but also ensures that scientifically reliable and well-documented information will be preserved and distributed with these aesthetically remarkable mineral specimens.

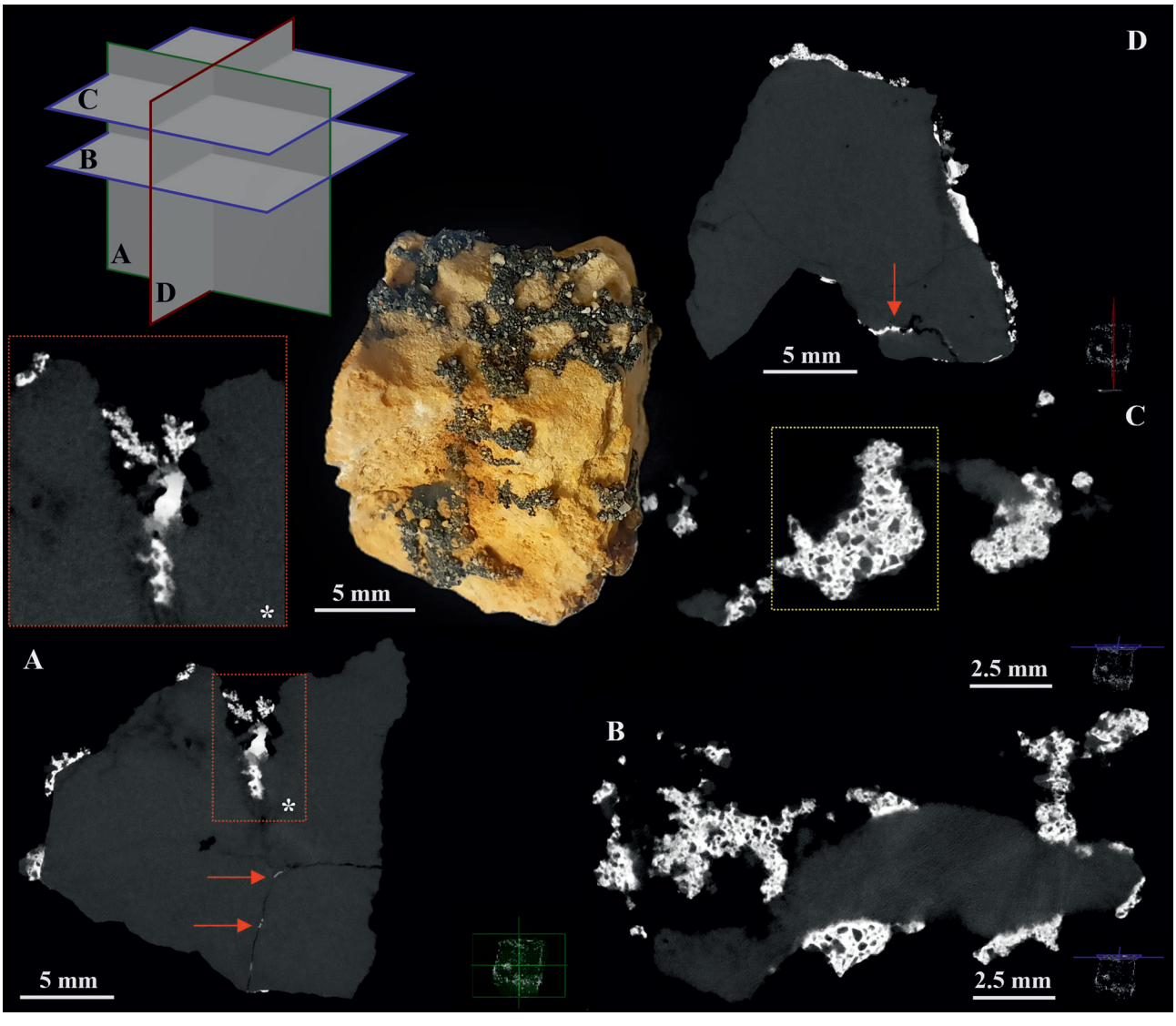

Figure 11. Computer tomography (CT) images from different directions of a ca. 1 cm^3 solid dolostone sample (dark) with manganese oxides (bright). Slice (A): 3D dendritic development in voids, slice (B) and (C): distribution of (dark) dolomite grains within the manganese-oxide matrix, slice (D): dolomite-free encrustation on the surface of the sample. Red arrows show manganese oxide penetrating the cracks of the specimen

11. ábra. *Különböző irányú CT-felvételek egy kb. 1 cm^3-es mangán-oxidos dolomitmintáról. (A): 3D-s dendrites kifejlődésű mangán-oxidok (világos), (B) és (C): dolomitszemcsék (sötét) eloszlása a mangán-oxidos mátrixban, (D): dolomitmentes mangán-oxidos bekérgezés a minta felszínén. A piros nyilak a mangán-oxidos repedéskitöltéseket mutatják*

Acknowledgement

The authors express their gratitude to Eszter Hegyesi and Tamás Németh for the samples provided for this research and for their enthusiasm, which made it possible to preserve these special specimens for the benefit of future research. Gratitude is also extended to the reviewers for the thorough evaluation of the manuscript and for their helpful and constructive comments and suggestions.

References – Irodalom

Babinszki E., Piros O., Budai T., Gyalog L., Halász A., Király E., Koroknai B., Lukács R. & M. Tóth T. 2023a: *Magyarország litosztratigráfiai egységeinek leírása I. Prekainozoos képződmények*. – Szabályozott Tevékenységek Felügyeleti Hatósága, Budapest, 275 p.

Babinszki E., Piros O., Csillag G., Fodor L., Gyalog L., Kercsmár Zs., Less, Gy., Lukács R., Sebe K., Selmeczi I., Szepesi J.& Sztanó O. 2023b: *Magyarország litosztratigráfiai egységeinek leírása II. Kainozoos képződmények*. – Szabályozott Tevékenységek Felügyeleti Hatósága, Budapest, 179 p.

Bernardini, S., Bellatreccia, F., Municchia A. C., Ventura, G. D. & Sodo, A. 2019: Raman spectra of natural manganese oxides. – *Journal of Raman Spectroscopy* **50**(6), 873–888. https://doi.org/10.1002/jrs.5583

Bernardini, S., Bellatreccia, F., Municchia A. C., Ventura, G. D. & Sodo, A. 2020: A reliable method for determining the oxidation state of manganese at the microscale in Mn oxides via Raman spectroscopy. – *Geostandards and Geoanalytical Research* **45**(1), 223–244. https://doi.org/10.1111/ggr.12361

Bernardini, S., Ventura, G. D., Mihailova B. & Sodo, A. 2024: The stability of manganese oxides under laser irradiation during Raman analyses: I. Compact Versus Channel Structures. – *Journal of Raman Spectroscopy* **56**(1), 95–112. https://doi.org/10.1002/jrs.6740

Bernardini, S., Ventura, G. D., Jovane, L., Sodo, A. & Mihailova B. 2025: The stability of manganese oxides under laser irradiation during Raman analyses: II. Layer structures. – *Journal of Raman Spectroscopy* **56**, 1072–1088. https://doi.org/10.1002/jrs.6829

Budai, T. & Vörös, A. 2006: Middle Triassic platform and basin evolution of the Southern Bakony Mountains (Transdanubian Range, Hungary). – *Rivista Italiana di Paleontologia e Stratigrafia* **112**(3), 359–371. https://doi.org/10.13130/2039-4942/6346.

Budai, T., Császár, G., Csillag, G., Dudko, A., Koloszár, L. & Majoros, G. 1999: Geology of the Balaton Highland. – *Occasional papers* **197**. Geological Institute of Hungary, Budapest.

Çalik, A. & Arzoğullari, U. 2014: Occurrence of dendritic agate from Dereyalak village (Eskişehir) – NW of Turkey and its relationship to sepiolite nodules in the region. – *Journal of African Earth Sciences* **97**, 99–108. https://doi.org/10.1016/j.jafrearsci.2014.04.028

Carmichael, S. K., Doctor, D. H., Wilson, C. G., Feierstein, J. & McAleer, R. J. 2017: New insight into the origin of manganese oxide ore deposits in the Appalachian Valley and Ridge of northeastern Tennessee and northern Virginia, USA. – *Geological Society of America Bulletin* **129**(9–10), 1158–1180. https://doi.org/10.1130/B31682.1

Dekoninck, A., Ruffet, G., Baptiste, J., Wyns, R., Philippo, S., Zhang, Y. & Namur, O. 2023: Petrogenesis and $^{40}Ar/^{39}Ar$ dating of hydrothermal romanèchite from the sub-aerial fault-related Romanèche Mn deposit (France). – *Chemical Geology* **618**, 121280. https://doi.org/10.1016/j.chemgeo.2022.121280.

Esteban, M., Budai, T., Juhász, E. & Lapointe, P. 2009: Alteration of Triassic carbonates in the Budai Mountains – a hydrothermal model. – *Central European Geology* **52**(1), 1–29. https://doi.org/10.1556/ceugeol.52.2009.1.1

Fodor, L., Héja, G., Kövér, S., Csillag, G. & Csicsek, Á. L. 2017: Cretaceous deformation of the south-eastern Transdanubian range unit, and the effect of inherited Triassic–Jurassic normal faults. Pre-conference field trip, CETeG – 15th meeting of the Central European Tectonic Studies Group. Zánka, Lake Balaton, Hungary. – *Acta Mineralogica-Petrographica, Field Guide Series* **32**, 47–76.

Haas, J., Budai, T., Csontos, L., Fodor, L. & Konrád, Gy. 2010: *Pre-Cenozoic geological map of Hungary. 1:500 000*. – Geological Institute of Hungary.

Héja G., Budai T. & Csicsek Á. 2024: Triász medence-geometria és fáciesváltozások hatása a Balaton-felvidék és a Veszprémi-fennsík eoalpi szerkezetalakulására. – *Földtani Közlöny* **154**(2), 239–256. https://doi.org/10.23928/foldt.kozl.2024.154.2.239

Hou, Z., Woś, D, Tschegg, C., Rogowitz, A., Rice, A. H. N., Lutz, N., Fusseis, F., Szymczak, P. & Grasemann, B. 2023: Three-dimensional mineral dendrites reveal a nonclassical crystallization pathway. – *Geology* **51**, 626–630. https://doi.org/10.1130/G51127.1

Hou, Z., Woś, D, Qiu, K-F., Rogowitz, A., Tschegg, C., Rice, A. H. N., Grasemann, B., Yu, H-C. & Szymczak, P. 2025: Mineral dendrites: Indicators for geological aqueous environments. – *Earth Science Reviews* **270**, 105231. https://doi.org/10.1016/j.earscirev.2025.105231

Julien, C. M., Massot, M. & Poinsignon, C. 2004: Lattice vibrations of manganese oxides: Part I. Periodic structures. – *Spectrochimica Acta Part A* **60**(3), 689–700. https://doi.org/10.1016/S1386-1425(03)00279-8

Kupi, L. 2021a: Neu aus Ungarn: Romanèchit-Dendriten. – *Lapis* **46**(3), 36–38.

Kupi L. 2021b: Új hazai lelet: romanèchit, goethit. – *Élet és Tudomány* **76**(12), 355.

Liu, C., Calo, V. M., Regenauer-Lieb, K. & Hu, M. 2023: Dendritic growth patterns in rocks: Inverting the driving and triggering mechanisms. – *Journal of Geophysical Research: Solid Earth* **128**, e2023JB027105. https://doi.org/10.1029/2023JB027105

Lafuente, B., Downs, R. T, Yang, H. & Stone, N. 2016: The power of databases: The RRUFF project. – In: Armbruster, T. & Danisi, R. M. (eds): *Highlights in Mineralogical Crystallography.* Berlin, München, Boston: De Gruyter, 1–30. https://doi.org/10.1515/9783110417104-003

Mozgai Zs. 2023: Világhíressé vált ásványlelet mentése, romanéchit, goethit a királyszentistváni dolomitbányából. – *Folia Musei Historico-naturalis Bakonyiensis* **40,** Zirc, 39–45.

Nagy B. 1979: A budai-hegységi porlott dolomitok ásvány-kőzettani, geokémiai és genetikai vizsgálata. – *Földtani Közlöny* **109**, 46–74.

Namgung, S. & Lee, G. 2025: Chemical and Structural Diversity of Manganese Oxides: Challenges and Advances in Characterization. – *Economic and Environmental Geology* **58**(6), 629–639. (in Korean with English abstract) https://doi.org/10.9719/EEG.2025.58.6.629.

Ng, T. F. & Teh, G. H. 2009: Fractal and shape analyses of manganese dendrites on vein quartz. – *Bulletin of the Geological Society of Malaysia* **55**, 73–79. https://doi.org/10.7186/bgsm55200912

Nicholson, K. 1992: Contrasting mineralogical-geochemical signatures of manganese oxides: guides to metallogenesis. – *Economic Geology* **87**, 1253–1264. https://doi.org/10.2113/gsecongeo.87.5.1253

Poros, Zs., Machel, H. G., Mindszenty, A. & Molnár, F. 2013: Cryogenic powderization of Triassic dolostones in the Buda Hills, Hungary. – *International Journal of Earth Sciences (Geologische Rundschau)* **102**, 1513–1539. https://doi.org/10.1007/s00531-013-0883-7

Post, J. E. 1999: Manganese oxide minerals: Crystal structures and economic and environmental significance. – *Proceedings of the National Academy of Sciences (PNAS)* **96**(7), 3447–3454. https://doi.org/10.1073/pnas.96.7.3447

Post, J. E., McKeown, D. A. & Heaney, P. J. 2020: Raman spectroscopy study of manganese oxides: Tunnel structures – *American Mineralogist* **105**(8), 1175–1190. https://doi.org/10.2138/am-2020-7390

Post, J. E., McKeown, D. A. & Heaney, P. J. 2021: Raman spectroscopy study of manganese oxides: Layer structures. – *American Mineralogist* **106**(3), 351–366. https://doi.org/10.2138/am-2021-7666

Potter, R. M. & Rossman, G. R. 1979: Mineralogy of manganese dendrites and coatings. – *American Mineralogist* **64**(11–12), 1219–1226.

Ralph, J., Bargen, D. V., Pavel, M., Zhang, J., Que, X., Prabhu, A., Morrison, S. M., Li, W., Chen, W. & Ma, X. 2025: Mindat.org: The open access mineralogy database to accelerate data-intensive geoscience research. – *American Mineralogist* **110**(6), 833–844. https://doi.org/10.2138/am-2024-9486

Robb, L. 2004: *Introduction to Ore-Forming Processes*. – Wiley–Blackwell, 384 p.

Swartzlow, C. R. 1934: Two dimensional dendrites and their origin. – *American Mineralogist* **19**(9), 403–411.

Szakáll S. & Fehér B. 2025: *Második kiegészítés a „Magyarország ásványai" című könyvhöz.* – Kézirat, Herman Ottó Múzeum, Miskolc, 24 p. http://geomania.hu/moasv/Moasv-2kieg-2025.pdf

Tari G. & Horváth F. 2010.: A Dunántúli-középhegység helyzete és eoalpi fejlődéstörténete a Keleti-Alpok takarós rendszerében: egy másfél évtizedes tektonikai modell időszerűsége. – *Földtani Közlöny* **140**(4), 483–510.

Topa, B. A., Papp, R. Z., Leskó, M. Zs., Váczi, T. & Weiszburg, T. G. 2018: Mineralogical and textural study of manganese oxides and oxyhydroxides related to the investigation of the Úrkút manganese deposit, Hungary. – In: *XXII. Meeting of the International Mineralogical Association: Book of Abstracts.* Melbourne, Australia 536 p., 480.

Turner, S. & Buseck, P. R. 1979: Manganese oxide tunnel structures and their intergrowths. – *Science* **203**(4379), 456–458. https://doi.org/10.1126/science.203.4379.456.

Turner, S. & Buseck, P. R. 1981: Todorokites: A new family of naturally occurring manganese oxides. – *Science* **212**, 1024–1027. https://doi.org/10.1126/science.212.4498.1024

Vasconcelos, P. M., Becker, T. A., Renne, P. R. & Brimhall, G. H. 1992: Age and duration of weathering by ^{40}K–^{40}Ar and $^{40}Ar/^{39}Ar$ analysis of potassium-manganese oxides. – *Science* **258**(5081), 451–455. https://doi.org/10.1126/science.258.5081.451

Vermeersch, E., Košek, F., De Grave, J., Jehlička, J., Vandenabeele, P. & Rousaki, A. 2023: Identification of tunnel structures in manganese oxide minerals using micro-Raman spectroscopy. – *Journal of Raman Spectroscopy* **54**(11), 1201–1212. https://doi.org/10.1002/jrs.6536

Xu, H., Chen, T. & Konishi, H. 2010: HRTEM investigation of trilling todorokite nano-phase Mn-oxides in manganese dendrites. – *American Mineralogist* **95**(4), 556–562. https://doi.org/10.2138/am.2010.3211

Wang, F., Zheng, Y., Chen, Q., Yan, Z., Lan, D., Lester, E. & Wu, T. 2024: A critical review of facets and defects in different MnO_2 crystalline phases and controlled synthesis – Its properties and applications in the energy field. – *Coordination Chemistry Reviews* **500**, 215537. https://doi.org/10.1016/j.ccr.2023.215537

Warr, L. N. 2021: IMA-CNMNC approved mineral symbols. – *Mineralogical Magazine* **85**(3), 291–320. https://doi.org/10.1180/mgm.2021.43

Manuscript received: 02/03/2026